

Magnetic reconnection in the Jovian tail: X-line evolution and consequent plasma sheet structures

S. Kasahara,¹ E. A. Kronberg,² N. Krupp,² T. Kimura,¹ C. Tao,¹ S. V. Badman,¹ A. Retinò,³ and M. Fujimoto¹

Received 30 May 2011; revised 8 August 2011; accepted 12 September 2011; published 22 November 2011.

[1] Magnetic reconnection in planetary magnetospheres plays important roles in energy and mass transfer in the steady state, and also possibly in transient large-scale disturbances. In this paper we report observations of a reconnection event in the Jovian magnetotail by the Galileo spacecraft on 17 June 1997. In addition to the tailward retreat of a main X-line, signatures of recurrent X-line formations are found by close examination of energetic particle anisotropies. Furthermore, detailed analyses of multi-instrumental data for this period provide various spatiotemporal features in the plasma sheet. A significant density decrease was detected in the central plasma sheet, indicative of the transition to lobe (open field line) reconnection from plasma sheet (closed field line) reconnection. When Galileo vertically swept through the plasma sheet, a velocity layer structure was observed. We also analyze a strong southward magnetic field which is similar to dipolarization fronts observed in the terrestrial magnetotail: the ion flow ($\sim 450 \text{ km s}^{-1}$) was observed behind the magnetic front, whose thickness of 10000–20000 km was of the order of ion inertial length. The electron anisotropy in this period suggests an anomalously high-speed electron jet, implying ion–electron decoupling behind the magnetic front. Particle energization was also seen associated with these structures. These observations suggest that X-line evolution and consequent plasma sheet structures are similar to those in the terrestrial magnetosphere, whereas their generality in the Jovian magnetosphere and influence on the magnetospheric/ionospheric dynamics including transient auroral events need to be further investigated with more events.

Citation: Kasahara, S., E. A. Kronberg, N. Krupp, T. Kimura, C. Tao, S. V. Badman, A. Retinò, and M. Fujimoto (2011), Magnetic reconnection in the Jovian tail: X-line evolution and consequent plasma sheet structures, *J. Geophys. Res.*, *116*, A11219, doi:10.1029/2011JA016892.

1. Introduction

[2] Jovian tail reconnection has been reported based on the observations of energetic particles and the magnetic field. For instance, with Voyager 2 data *Nishida* [1983] showed the simultaneity of anti-sunward energetic particle bursts and northward magnetic field spikes. Although only a few observations had been obtained during the “flyby” era (Pioneer, Voyager, and Ulysses), the first orbiting satellite Galileo collected a significant amount of evidence for tail reconnection. *Russell et al.* [1998] reported strong vertical (north-south) magnetic field events (SVM events) and attributed them to localized transient reconnection. *Woch et al.* [2002] statistically studied the anisotropy of energetic particle bursts and deduced the typical X-line location, which is at

$\sim 70 R_J$ in the postmidnight sector and $\sim 120 R_J$ in the midnight sector. A similar result on the X-line location was obtained through the statistical analyses on the vertical component of the magnetic field [*Vogt et al.*, 2010], based on the assumption that prominent southward and northward magnetic field components are accompanied by radially inward and outward plasma flow, respectively. Furthermore, time series analyses of energetic particle data have also shown that the X-line often retreats tailward [*Krupp et al.*, 1998; *Woch et al.*, 1999; *Kronberg et al.*, 2005].

[3] Obviously far more knowledge has been accumulated for magnetic reconnection in the Earth’s magnetosphere. A significantly larger amount of high-time resolution data (compared to the Jupiter observations) and multispacecraft investigations have revealed steady and transient structures in the plasma sheet during reconnection events.

[4] For instance, velocity layer structures in the plasma sheet boundary layer (PSBL) through the inner plasma sheet have been seen in the energetic particle data associated with reconnection [e.g., *Scholer et al.*, 1986; *Onsager et al.*, 1991; *Sarafopoulos et al.*, 1997]. Particles launched around the X-line propagate along the magnetic field line, and at the same time the flux tube is convected equatorward. As a result,

¹Institute of Space and Astronautical Science, Japan Aerospace Exploration Agency, Sagami-hara, Japan.

²Max-Planck-Institut für Sonnensystemforschung, Katlenburg-Lindau, Germany.

³Laboratoire de Physique des Plasmas-CNRS, Observatoire de Saint-Maur, Saint-Maur-Des-Fossés, France.

the particles with the higher (lower) velocity are concentrated on the region away from (close to) the plasma sheet center if they are detected far from the X-line.

[5] Dipolarization of the nightside magnetic field is one of the most significant consequences of tail reconnection since it is deeply related to auroral substorms [e.g., *Baker et al.*, 1996]. Based on a superposed epoch analysis using Geotail data, *Ohtani et al.* [2004] deduced the average picture of dipolarization events; the vertical magnetic field component shows a dip before the dipolarization peak, and the density decreases after the dipolarization peak. These signatures are well reproduced by the full-particle simulation by *Sitnov et al.* [2009]. Furthermore, the planetward propagation of the dipolarization front (DF) has been clearly captured by THEMIS multispacecraft observations [*Runov et al.*, 2009, 2011a]. Their case-study shows the averaged signatures of dipolarization mentioned above. Then *Runov et al.* [2011b] conducted a multievent study using THEMIS data. In addition to the average picture similar to the previous study [*Ohtani et al.*, 2004], they showed an intense electric field in the dawn-to-dusk direction as well as the normal direction (mainly Earthward) and also discussed the kinetic structure of DF.

[6] The earthward propagating DF is important from the view point of particle acceleration [*Sergeev et al.*, 2009]. The strong magnetic field within a DF can lead to the acceleration of charged particles via the betatron mechanism [e.g., *Ashour-Abdalla et al.*, 2011].

[7] Apart from propagating DFs, particle accelerations at and around the X-line have also been observed [e.g., *Terasawa and Nishida*, 1976; *Øieroset et al.*, 2002; *Ásnes et al.*, 2008; *Chen et al.*, 2008; *Retinò et al.*, 2008]. Although intensive simulation studies have proposed several acceleration mechanisms to explain observed signatures [*Hoshino et al.*, 2001; *Hoshino*, 2005; *Pritchett*, 2006; *Drake et al.*, 2006; *Oka et al.*, 2010], the importance of each mechanism is not yet quantitatively understood.

[8] Returning to Jupiter, some morphological features have been revealed by Galileo observations (e.g., typical X-line location and motion), whereas structures inside the active plasma sheet (i.e., when reconnection is ongoing) have not been sufficiently resolved. One interesting aspect of the study on the Jovian plasma sheet is that plasma parameters and the scale size of the magnetosphere are significantly different from the terrestrial case. Observations in such a different parameter space would provide significant clues to enhance our understanding on common plasma processes. Another interesting issue in the Jovian tail is the significance of lobe reconnection. Thus far there has been no agreement on the importance of the Dungey-cycle, which includes lobe (open field line) reconnection in the tail [*McComas and Bagenal*, 2007; *Cowley et al.*, 2008]. In addition to such a steady state issue, it is also interesting whether lobe reconnection triggers distinctive auroral phenomena as argued in the terrestrial case [*Baker et al.*, 1996; *Russell*, 2000]. Observational evidence of lobe reconnection in the Jovian tail, however, has not been well documented in previous studies.

[9] In this paper we study the Jovian plasma sheet in one of the reconnection events listed by *Kronberg et al.* [2005] in detail. In order to address the plasma structure in the active plasma sheet and to identify lobe reconnection, we utilize data

of energetic particles, magnetic field, and electron density, which have rarely been used in concert for the study on the Jovian tail.

2. Methodology

2.1. Instruments

[10] In this work we use data from Energetic Particle Detector (EPD) [*Williams et al.*, 1992] on board Galileo. This instrument consists of two telescopes: Composition Measurement System (CMS) for ion fluxes (80–1250 keV for protons, 12–562 keV/nuc for oxygen ions, and 16–310 keV/nuc for sulfur ions) and Low-energy Magnetospheric Measurement System (LEMMS) for the electron (15–884 keV) and species-integrated ion (22–12400 keV) fluxes.

[11] Data are accumulated within sampling times of ~ 1.5 min (for the data set analyzed here) and the instruments cover an almost full-sphere, which is divided into 16 or 6 sectors. In this study we mainly analyze 16-sector resolution data, whereas we also use 6-sector data if needed, since 16-sector data are available for fewer energy channels.

[12] Particle pitch angles (PAs) are determined with the magnetic field data obtained by the Galileo magnetometer (MAG) [*Kivelson et al.*, 1992]. We discuss PAs only when the magnetic field direction is stable during a sampling time, since otherwise the PA determination is unreliable. The time resolution of the MAG instrument for our event is 24 s. The magnetic field vector components in system-III coordinates form the standard right-handed spherical triad (r , θ , ϕ). B_r is along the Jupiter to spacecraft line, positive away from Jupiter. B_ϕ is parallel to the Jovigraphic equator (positive in the corotation direction), and B_θ completes the right-handed set (positive southward).

[13] In addition to these two instruments, the plasma wave subsystem (PWS) [*Gurnett et al.*, 1992] is utilized to deduce the electron density, assuming that the sharp cutoff of the broadband continuum corresponds to the in-situ plasma frequency [e.g., *Kurth*, 1992].

2.2. Energetic Particle Anisotropy

[14] Energetic particle anisotropy is calculated using EPD flux data, which are functions of particle energy, turntable angle, and spin phase angle. The 16-sector flux data are fitted by the least square method with the spherical harmonic function:

$$J(E, \alpha, \beta) = \sum_{n=0}^{\infty} \sum_{m=-n}^n A_{nm}(E) Y_{nm}(\alpha, \beta), \quad (1)$$

$$Y_{nm}(\alpha, \beta) = \begin{cases} P_{nm}(\cos \alpha) \cos(m\beta) & m > 0, \\ P_{n|m|}(\cos \alpha) \cos(|m|\beta) & m < 0, \end{cases} \quad (2)$$

where P_{nm} is the associated Legendre function. E , α , and β are the particle energy, polar angle, and azimuthal angle, respectively. Coefficients $A_{nm}(E)$ are referred to as the n th-order anisotropies. In this study the magnetic field direction is defined as the pole for the definition of α and β . When the fluctuation of magnetic field direction during an EPD time bin is large, we instead adopt the spacecraft spin axis as the pole. In the former case, we calculate the zeroth-, first-,

and second-order anisotropies: A_{00} , A_{1-1} , A_{10} , A_{11} and A_{20} , with setting other coefficients to be zero. In such a case equation (1) reduces to

$$J(E) = A_{00}(E) + A_{10} \cos \alpha + A_{11} \sin \alpha \cos \beta + A_{1-1} \sin \alpha \sin \beta + A_{20} (3 \cos^2 \alpha - 1)/2. \quad (3)$$

When A_{20} is positive (negative), the flux tends to be more intense in the parallel/anti-parallel (perpendicular) direction to the magnetic field, and we refer to such PA anisotropies as bi-directional (pancake). It should be noted, however, that A_{20} is not a robust index of bi-directional or pancake types (for instance, it is possible that mono-directional beam is best fitted by the superposition of A_{10} and positive A_{20} , depending on the flux angular distribution). Therefore we check not only A_{20} but also the PA distributions when we discuss bi-directional or pancake distributions.

[15] In the case of using the spin axis pole, we calculate only the zeroth- and first-order anisotropies. In both cases, the first-order anisotropies are converted into system-III coordinates, resulting in A_{1r} , $A_{1\theta}$, and $A_{1\phi}$ (radial, meridional, and corotational directions, respectively), and therefore the only difference between using the magnetic field pole and the spin axis pole is that the latter does not provide the second-order anisotropies.

[16] As has been often assumed in many previous studies [e.g., *Nishida*, 1983; *Woch et al.*, 2002; *Kronberg et al.*, 2005], we use the energetic particle anisotropy in the tail to infer the location of tail reconnection. Although the ion anisotropy may also be explained by other mechanisms, the accompanied detection of the field-aligned streaming electrons supports the above interpretation [*Grigorenko et al.*, 2009; *Kronberg et al.*, 2011].

[17] When the flow velocity V is much lower than the detected particle velocity v and the anisotropy is purely due to the bulk flow (i.e., the contributions from the pressure gradient and PA anisotropy are negligible), the flow vector \mathbf{V} can be calculated through

$$\mathbf{V} = \frac{v}{2 + a\gamma} \mathbf{A}_1, \quad (4)$$

$$a \equiv \frac{E + 2mc^2}{E + mc^2}, \quad (5)$$

where $\mathbf{A}_1 = (A_{1r}, A_{1\theta}, A_{1\phi})$, v is the particle velocity of the corresponding energy channel, $\gamma = -d(\log J)/d(\log E)$ is the spectral index around the corresponding energy channel, m is the particle mass, and c is the light speed [*Forman*, 1970; *Birmingham and Northrop*, 1979]. For ions analyzed here $a \sim 2$, whereas for the high-energy electrons $a < 2$. The above equation for the flow velocity can be applied to each species and each energy channel of EPD, which allows a consistency check for the assumptions.

3. Overview of the Reconnection Event

[18] Figure 1 shows the overview of the reconnection event on 17 June 1997 as seen by Galileo, which was located at a distance of $\sim 75 R_J$ from Jupiter and a local time of ~ 2.5 h. The plotted time period is ~ 21 h. Magnetic field data in the bottom

panel (Figure 1f), which is running-averaged over the EPD sampling time, illustrate the spacecraft location relative to the plasma sheet center (i.e., where the radial component of the magnetic field B_r reverses sign). During this period Galileo experienced the northern side of the plasma sheet ($B_r > 0$) and the southern side ($B_r < 0$) alternately, due to the plasma sheet flapping caused by the planetary rotation.

[19] The electron density derived from the cutoff frequency of the continuum (Figure 1a, sharp transition between green and yellow guided by black dots) and energetic particle flux (Figures 1b and 1c) show drastic increases and decreases during this period, indicative of an active plasma sheet. Furthermore, the radial anisotropy (A_{1r}) of energetic electrons (304–527 keV) and ions (65–120 keV), which are shown in Figures 1d and 1e (normalized by A_{00}), respectively, roughly illustrate tailward streaming (until ~ 04 UT, a blue bar in the middle of Figure 1) followed by Jupiterward streaming (from ~ 07 UT, a red bar in the middle of Figure 1). In the paper by *Kronberg et al.* [2005], this event (over ~ 13 h) is listed as one of the reconnection events and the anisotropy reversal is attributed to the tailward retreat of the X-line passing through Galileo.

[20] Putting aside the energetic particle anisotropy, another remarkable feature is the low electron density. In particular, we interpret the shaded regions as the magnetic lobe (i.e., magnetic field lines are open) partly with PSBL, judging from the extremely low electron density ($< 10^{-3} \text{ cc}^{-1}$) as well as the low level of the energetic particle fluxes [cf. *Woch et al.*, 1999; *Russell et al.*, 2000]. Such low density is not observed in quiet conditions (e.g., on the next day of the present event, not shown); Galileo normally stays in the closed field line region, where the typical electron density is $\sim 10^{-2} \text{ cc}^{-1}$ [cf. *Louarn et al.*, 2000; *Frank et al.*, 2002]. Therefore the plasma sheet during this event seems to have been thinner than during the quiet time, which is qualitatively consistent with the occurrence of reconnection.

[21] Among a number of bursty events (based on EPD and MAG data), we have selected this event since it contains various plasma sheet signatures associated with tail reconnection in which particle anisotropies with regard to the magnetic field can be discussed more unambiguously compared to other events. In the following sections, we examine this event in more detail with electron density, energetic particle, and magnetic field data and discuss plasma structures embedded in the active plasma sheet. The time periods analyzed below are indicated in the top of Figure 1 with green bars and characters A-E.

4. Reconnection Locations Deduced From Particle Anisotropies

4.1. Period A: Closed Field Line Reconnection

[22] Figure 2 shows the zoom-in data of period A (0045–0220 UT). Electron density (Figure 2a, visually recognized as the sharp transition between green and yellow which corresponds the lower cutoff frequency of the continuum), energetic particle anisotropies (Figures 2b–2f), and the magnetic field (Figure 2g) are plotted. The meridional anisotropy ($A_{1\theta}$) is not displayed since generally it is much smaller than A_{1r} and $A_{1\phi}$. From before 0100 to 0140 UT, the first-order radial anisotropies (A_{1r}) of the electrons (Figures 2b and 2c) were negative (i.e., Jupiterward streaming). In addition, the

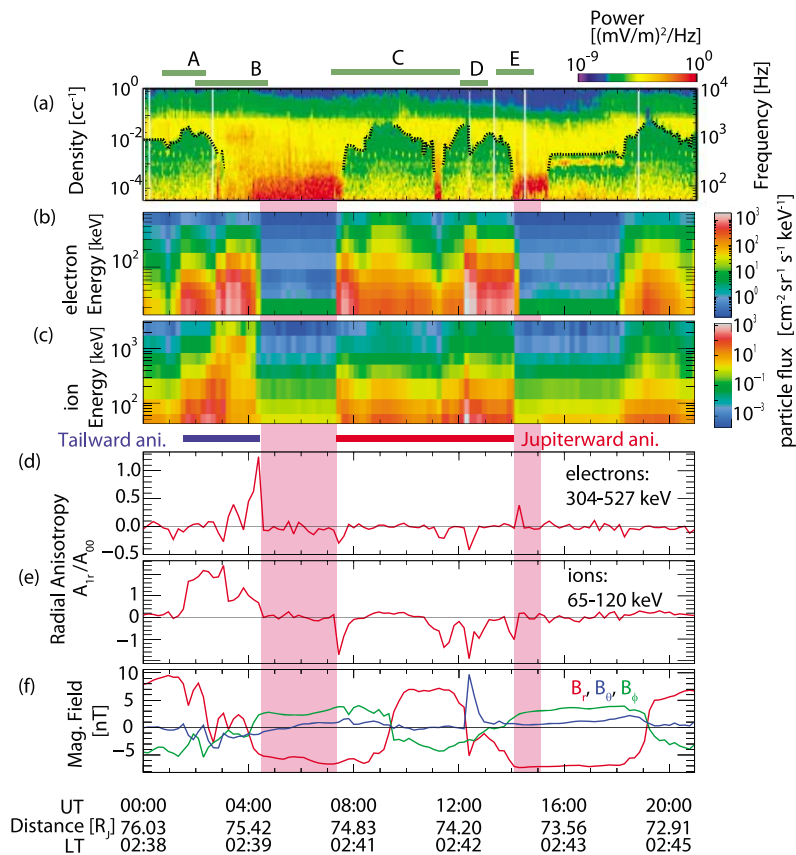


Figure 1. Overview of the Galileo observations on 17 June 1997. (a) Frequency-time spectrogram of the electric field (the cutoff of the continuum is indicated by black dots drawn by hand). (b, c) Energy-time spectrogram of electrons and ions (no mass discrimination), respectively. (d, e) Radial anisotropies of electrons and ions, respectively. (f) Magnetic field in system-III coordinates. Magenta shading indicates the lobe region (partly including plasma sheet boundary layer).

negative correlation between A_{1r} and $A_{1\phi}$ reflecting the B_r - B_ϕ relation indicates these electrons are field-aligned. The Jupiterward-streaming field-aligned electrons are considered to have come from the reconnection site, thus placing the X-line tailward of Galileo at this time. As suggested by the significantly positive A_{20} (bi-directional anisotropy), there also existed the tailward streaming field-aligned electrons in addition to the dominant Jupiterward electrons. These tailward electrons may be those which were originally Jupiterward streaming and mirror-reflected or looped back along the closed magnetic field. It is also possible that these were originally launched from another X-line Jupiterward of Galileo.

[23] After 0141 UT, B_θ showed a negative excursion while $|B_r|$ decreased. The polarity change of B_θ component (from positive to negative) suggests the tailward transit of an O-line (with another X-line Jupiterward of Galileo). Although the B_θ variation alone may also be interpreted as the wave-like structure of the plasma sheet [Jackman *et al.*, 2009], the tailward anisotropies ($A_{1r} > 0$) of the electrons and ions support the X-line existence Jupiterward of Galileo. Another possible interpretation for the observed polarity change of B_θ is the Jupiterward motion of the X-line passing over Galileo.

However, the former interpretation (i.e., O-line tailward motion) is more likely, since the predominant ion tailward anisotropies at ~ 0130 UT are inconsistent with the Jupiterward-moving X-line located tailward of Galileo. The particle anisotropies and our interpretation are schematically illustrated in Figure 3a.

[24] It is important to note here that the anisotropies were observed within the relatively high density plasma sheet ($\sim 10^{-2}$ cc $^{-1}$). This fact indicates that magnetic reconnection proceeded inside the plasma sheet (i.e., closed field line reconnection) at this stage.

4.2. Period B: Open Field Line Reconnection

[25] Figure 4 represents the density, energetic particle anisotropies, and the magnetic field for period B (0200–0445 UT). A_{20} is not presented here due to the large magnetic field perturbation (directional change within an EPD time bin was often $>50^\circ$ from 0130 to 0430 UT). As can be seen in the reversal of B_r , Galileo was first on the northern side of the current sheet and then moved to the southern side. The radial anisotropies (A_{1r}) were almost persistently positive throughout this period (Figures 4b–4f), indicating the X-line was Jupiterward of Galileo. The X-line Jupiter-

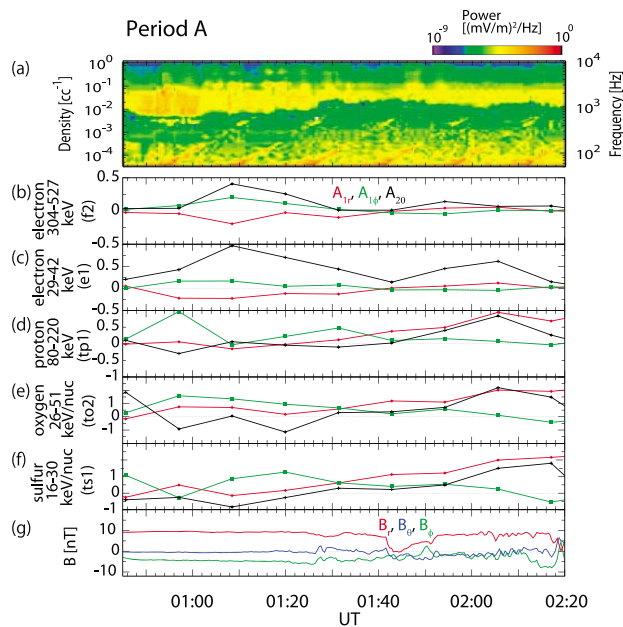


Figure 2. Integrated plot for period A. (a) Frequency-time spectrogram for the electron density estimation (the density can be recognized as the lower cutoff of the continuum, which corresponds to the sharp transition between green and yellow: at $\sim 10^{-2} \text{ cc}^{-1}$ for this period). (b–f) Energetic particle anisotropies (black: A_{20} , red: A_{1r} , green: $A_{1\phi}$; all anisotropies are normalized by A_{00}). (g) The magnetic fields are displayed.

ward of Galileo is also supported by the significant negative B_{θ} (Figure 4g). Several transient southward turnings (0215–0235 UT) imply the tailward passages of magnetic islands and/or wave-like structure of the plasma sheet.

[26] From ~ 0215 to 0415 UT, Galileo was located in the central plasma sheet since $|B_r|$ was very small (less than 5 nT for most times) and the sign changed several times. Nevertheless, the electron density started to decrease at ~ 0240 UT and became significantly lower than 10^{-2} cc^{-1} . This suggests the initiation of lobe reconnection (i.e., open field line reconnection). Lobe reconnection is also suggested by the sharp dropout of energetic particle fluxes seen at ~ 0435 UT (Figures 1b and 1c). The flux decrease of the energetic particles at the edge of the current sheet is more gradual in the quiet state. In contrast, the steep flux gradients at the edge of the current sheet, which are seen at ~ 0435 UT (and also in later periods, 0730 and 1420 UT), indicate that the lobe magnetic field lines were rapidly being fed into the reconnection outflow region. Further evidence for lobe reconnection is the decrease of the ambient horizontal magnetic field (B_r and B_{ϕ}), since it indicates the consumption of the magnetic energy stored in the lobe [cf. Baker *et al.*, 1996]. The absolute value of B_r was >8 nT at 00–01 UT (northern plasma sheet), and the value decreased down to ~ 5 nT by 0435 UT (southern lobe). The absolute value of B_{ϕ} similarly decreased compared to that at 00–01 UT.

[27] The observed signatures in period B are depicted in Figure 3b. Note that the schematic illustrates the plasma sheet after the initiation of lobe reconnection and hence magnetic islands and wavy structures which may have encountered

before lobe reconnection are not drawn. The spatial distribution of energetic particles in this period is further studied later.

4.3. Period C: Retreat of X-line

[28] Galileo moved back from the lobe to the southern plasma sheet at ~ 0730 UT (Figure 5a, and see also Figures 1a–1c). The Jupiterward anisotropies ($A_{1r} < 0$) of electrons and ions at 0725–0800 UT in Figures 5b–5f represent the X-line displacement to tailward of Galileo.

[29] Judging from the magnetic field data (Figure 5g), Galileo crossed the current sheet at ~ 0920 UT. Then the spacecraft grazed the northern PSBL edge at ~ 1100 –1120 UT, as identified by the dropout of the electron density and the magnetic field increase. The flux levels of the energetic particles are also low in this PSBL period (Figures 1b and 1c). After 1130 UT, Galileo moved back to the plasma sheet center.

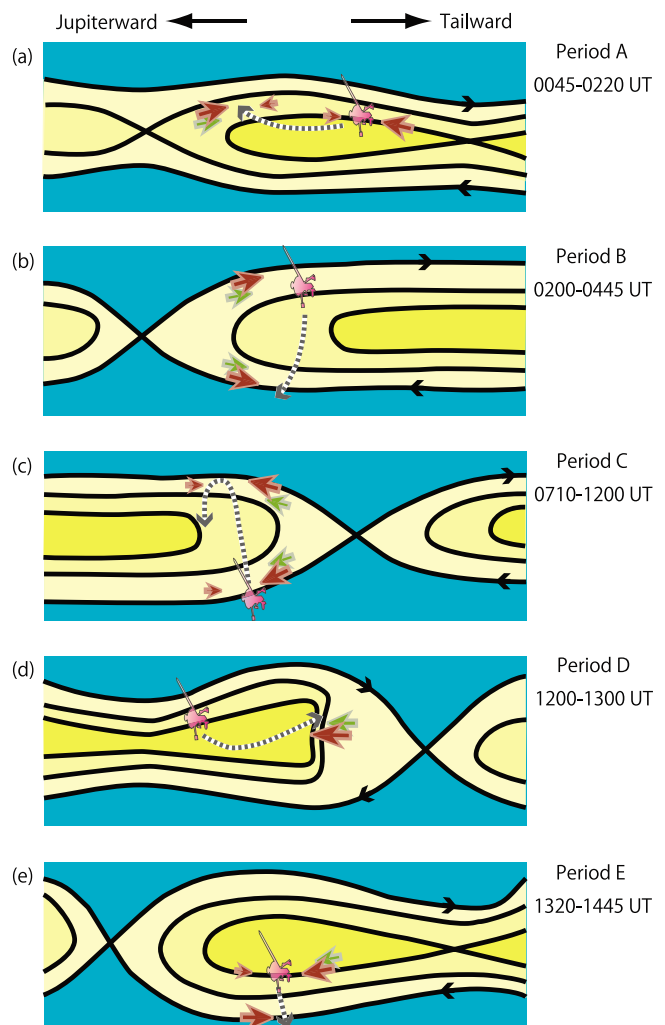


Figure 3. Schematic pictures of the electron anisotropy (brown arrows), the ion anisotropy (green arrows), and the spacecraft motion (gray broken arrows) relative to the X-lines. Blue regions are the magnetic lobe. Distance of Galileo spacecraft from Jupiter was $\sim 76 R_J$ and $\sim 74 R_J$ during period A and E, respectively.

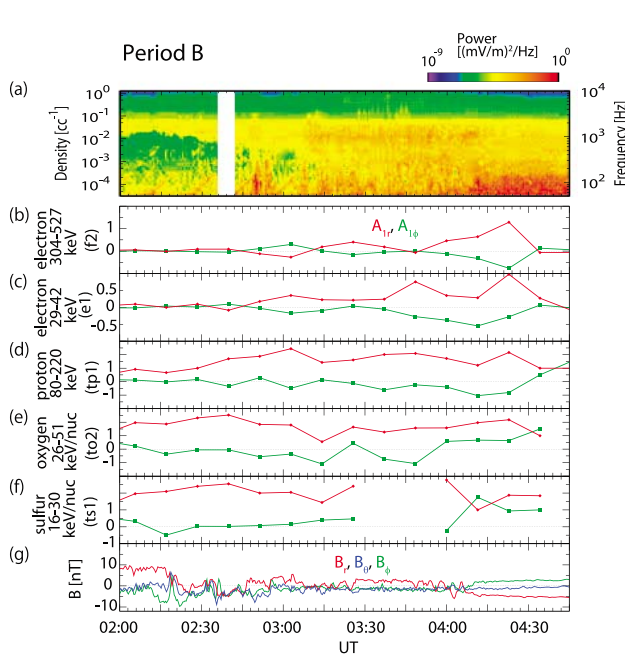


Figure 4. Integrated plot for period B. The format is the same as Figure 2, except for the absence of the second-order anisotropy.

[30] From 0830 to 1045 UT, no significant radial anisotropies are seen for any species and instead corotational anisotropies were dominant for ions (Figures 5d–5f), which is typical of the quiet state plasma sheet [Krupp et al., 2001]. In addition, the density is rather high compared to period B. These facts suggest that reconnection might have ceased and the dense plasma sheet recovered temporarily.

[31] However, lobe reconnection is indicated at least when the spacecraft crossed the southern PSBL (~ 0730 UT), where significant field-aligned anisotropies were detected, since the energetic particle flux gradient was very sharp and the electron density was very low. In addition, it is evident from the anisotropies that some activity recovered after 11 UT. The observations of reconnection signatures in this period are illustrated in Figure 3c. In association with the Jupiterward anisotropies, oppositely streaming minor electrons also existed as implied by the significant second-order anisotropies (i.e., $A_{20} > |A_{1r}|$). These electrons are interpreted to be the mirror-reflected components.

4.4. Period D: Reconnection Enhancement

[32] Data for period D (from 12–13 UT) are shown in Figure 6. This period includes an SVM event, for which the anomalously strong southward magnetic field has been reported [Russell et al., 1998]. The steep increase of the vertical magnetic field, its gradual relaxation, and precursor negative dip (Figure 6g) are quite similar to the DF signatures often observed in the Earth’s magnetosphere [Runov et al., 2009, 2011a, 2011b] and reproduced by numerical simulations [Sitnov et al., 2009].

[33] In addition to the previously reported magnetic field data, here we plot the electron density (Figure 6a) and energetic particle anisotropies (Figures 6b–6f). The density increased in front of the SVM, and then decreased signifi-

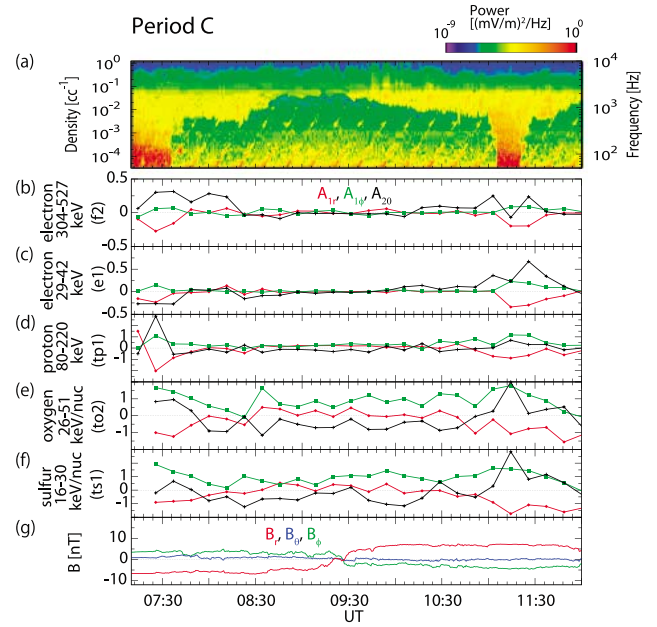


Figure 5. Integrated plot for period C. The format is the same as Figure 2.

cantly after a data gap. These signatures are also similar to the Earth’s dipolarization events and simulation results.

[34] For this event, the magnetic field is dominated by the B_θ component, while the ion anisotropies are dominated by the radial and corotational components. This suggests that the

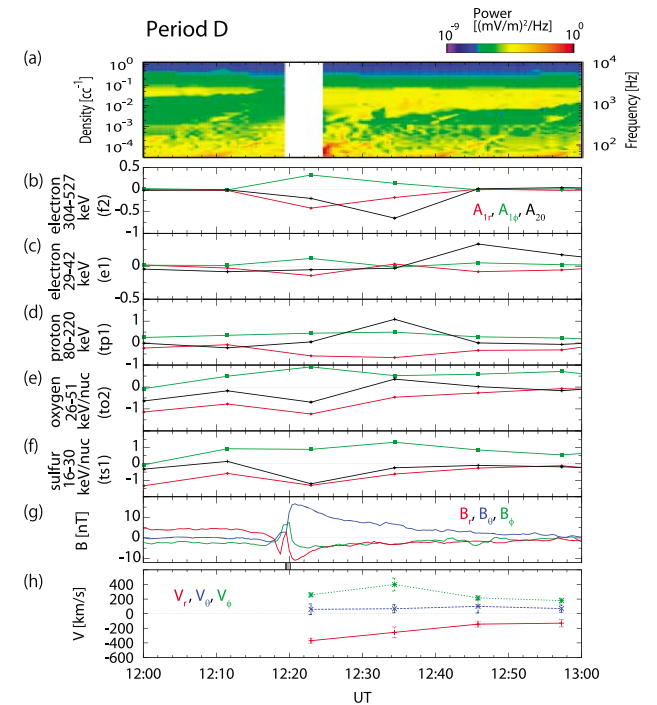


Figure 6. (a–h) Integrated plot for period D. The format is the same as Figure 2, except for the addition of the ion flow velocity in Figure 6h. Gray bars (narrow and thick) between Figures 6g and 6h indicate the period of sharp B_θ increase.

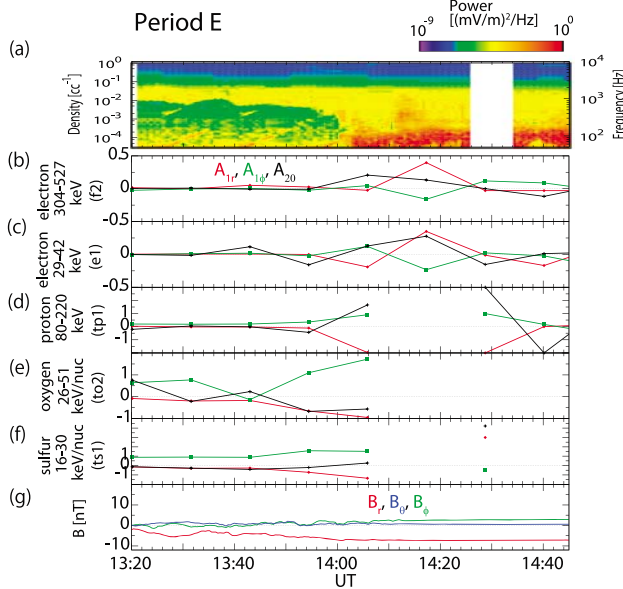


Figure 7. Integrated plot for period E. The format is the same as Figure 2.

anisotropy was due to the ion flow perpendicular to the magnetic field. The velocities calculated from these anisotropies via equation (4) for each ion species and energy channel are in agreement with each other, indicating that the velocities are reliable, and supporting the above expectation. Figure 6h shows the flow velocity averaged over the ion energies/species shown in Figures 6d–6f and other proton and oxygen channels (tp2 and to1). The error bar represents the standard deviation. The velocity is shown only for the B_θ -dominant period. The ion flow velocity was about $\sim 450 \text{ km s}^{-1}$ at/around the B_θ peak, and it decreased along with the B_θ decay. Such a flow signature is again consistent with the dipolarization pictures around the Earth.

[35] Another interesting feature, that is, the Jupiterward electron anisotropies at/behind the SVM front (perpendicular to the magnetic field) seen in Figures 6b and 6c, are analyzed later in detail. The spacecraft motion and particle anisotropies in this period are illustrated in Figure 3d.

4.5. Period E: A New X-line

[36] The last period E (1320–1445 UT) is shown in Figure 7. As can be seen in the magnetic field data (Figure 7g), Galileo was south of the current sheet throughout this period. After period D, the plasma sheet activity seems to have decreased, since any clear radial and bi-directional anisotropies are not seen until ~ 1345 UT. From ~ 1345 UT, however, Jupiterward anisotropies ($A_{1r} < 0$) are seen for electrons and ions, indicating the revival of reconnection tailward of Galileo.

[37] The most important signature here is the tailward anisotropies ($A_{1r} > 0$) at the edge of the plasma sheet (~ 1417 UT) seen only for the electrons (Figures 7b and 7c). These features are evidence of a new X-line Jupiterward of Galileo, as illustrated in Figure 3e. The energetic particle flux dropped sharply at the PSBL, again indicating lobe reconnection. After this lobe excursion, the plasma sheet became

quiet, and the energetic particle flux gradient became diffusive at least by 18 UT (see Figure 1).

5. Structures in the Active Plasma Sheet

[38] In the previous section we presented the X-line evolution, which is summarized in Figure 3. In a macroscopic view, the main X-line retreated tailward and a new X-line was formed Jupiterward of Galileo, although reconnection seems to have weakened or ceased intermittently. In addition to these large-scale activities, we also found quasi-stable structures and transient phenomena in the active plasma sheet. In this section we demonstrate the velocity layer structure in period B as well as the electron jet signature in period D (SVM event) and also discuss the particle accelerations in both periods.

5.1. Layering Structure: Velocity Filter Effect

[39] Figure 8 shows the energetic particle flux and the magnetic field in period B. The green and purple horizontal bars indicate when Galileo was in the inner and outer plasma sheet, respectively, judged from the magnetic B_r component. At first Galileo was in the northern outer plasma sheet. At ~ 0220 UT Galileo moved to the inner plasma sheet, where the sign of B_r reverses several times. From ~ 0315 UT Galileo moved back to the outer plasma sheet (B_r sign reversal is less frequent). At ~ 04 UT there was a current sheet crossing, and then Galileo moved to the southern outer plasma sheet.

[40] In Figures 8a and 8b omni-directional flux data are aligned in the order of the particle velocity from top to bottom. Vertical broken lines are put every 30 min for visual aid. In Figure 8a, the velocity layer structure is clearly seen; the lower-velocity particles were confined in the inner region before 03 UT and the higher-velocity particles increased in the outer region (after 03 UT). The absence of the higher-velocity ions in the outer region before 0220 UT would be due to the rapid sweep (i.e., Galileo moved to the inner region so rapidly that the accumulation time in the outer layer was short). A similar signature is also seen in Figure 8b. Again lower-velocity ions concentrated on the inner region whereas higher-velocity particles are more evident before Galileo penetrated into the inner plasma sheet. Although the peak of the ts1 channel (sulfur, 16–30 keV/nuc) shows a slight outward shift (Figure 8b, bottom), it should be noted that the counts are so low (only a few counts in some sectors and no counts in other sectors in one sampling time) that we cannot discuss the peak position unambiguously. The layer structure was missed in the southern PSBL (after ~ 0405 UT), again probably due to the rapid crossing.

[41] Such velocity layer structures associated with magnetic reconnection are well known for the Earth's magnetosphere [Scholer et al., 1986; Onsager et al., 1991; Sarafopoulos et al., 1997].

5.2. Structure of SVM

[42] The ion flow velocity was $\sim 450 \text{ km s}^{-1}$ at/behind the SVM structure. It is comparable to the Alfvén velocity V_A of 650 km s^{-1} , for which the electron density and the magnetic field were assumed to be $n_e \sim 0.003 \text{ cc}^{-1}$ and $B \sim 5 \text{ nT}$, respectively ($V_A = B/\sqrt{4\pi n_e e m_i/q}$). We also assumed the ion mass-per-charge to be $m_i/q \sim 10m_p/e$, where m_p and e are the proton mass and elementary charge (i.e., considering O^{2+}

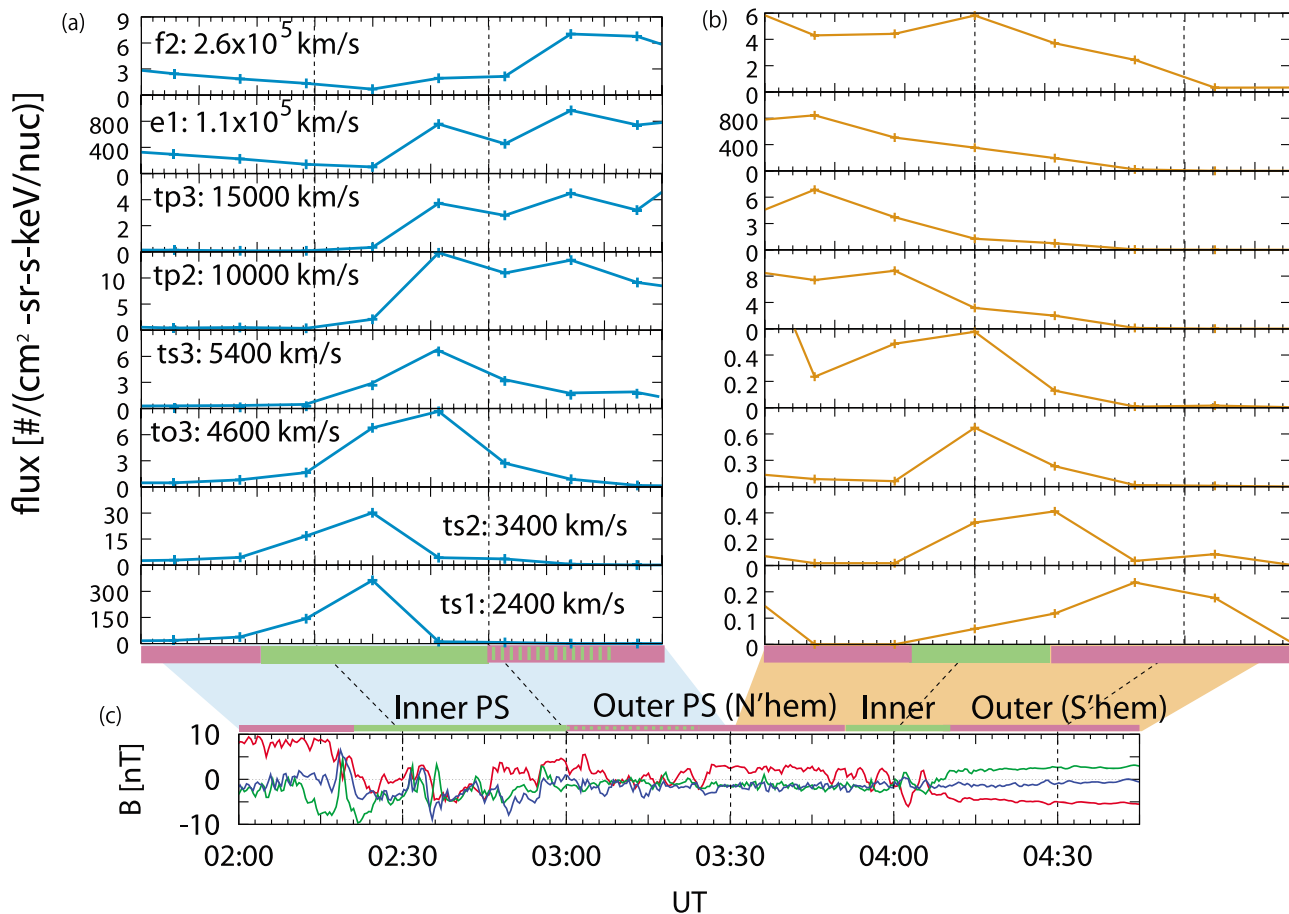


Figure 8. Omni-directional particle fluxes (a) for 0200–0330 UT and (b) for 0330–0415 UT and (c) the magnetic field data. Channels f2 and e1 are of electrons, and others are of ions. Galileo’s location inferred from the magnetic field is illustrated by purple and green bars. The inner plasma sheet (inner PS), the outer plasma sheet (outer PS) in the northern hemisphere (N’hem), and the outer plasma sheet in the southern hemisphere (S’hem) are shown.

and S^{3+} [cf. *Geiss et al.*, 1992]). Note that we cannot reject the possibility of other values, such as $m/q \sim 16m_p/e$ (i.e., O^+ and/or S^{2+}) due to the lack of mass and charge state information of low-energy ions for this event (for instance, significant amount of ions of $m/q \sim 16m_p/e$ are detected in some regions [*Frank et al.*, 2002]). Hence in our estimation including m and/or q , hereafter we accept an uncertainty of a factor up to ~ 2 . For instance, $V_A \sim 500$ km s⁻¹ for $m/q \sim 16m_p/e$ with the above density and the magnetic field.

[43] Since the duration of the steep increase of B_θ (indicated by gray bars between Figures 6g and 6h) was 36 ± 12 s (the large uncertainty is due to the sampling time of 24 s), the front thickness is estimated to be ~ 10000 – 20000 km, assuming the front structure moved with the ion flow velocity. The origin of this current layer will be discussed later.

5.3. Electron Jet Signature Associated With SVM

[44] Here we analyze the electron anisotropy in the period D in more detail. Associated with the SVM signature, significant electron anisotropy (especially A_{1r}), which peaked at data points at ~ 1223 UT, is seen in Figure 6. This anisotropy is perpendicular to the magnetic field, which is uncommon, since the field-perpendicular flow of electrons is generally much less evident in anisotropy than those of ions due to the

higher thermal velocity (equation (4)) [see also *Krimigis and Roelof*, 1983]. Therefore, the obtained anisotropies of the electrons suggest the unusually high-speed electron flow perpendicular to the magnetic field.

[45] Sector plots (angle-angle plots) for electron fluxes (Figure 9) provide more direct and detailed information on the electron anisotropy. Figure 9 illustrates the 16-sector data of the electrons (e1: 29–42 keV and f2: 304–527 keV) for two successive time bins (1217:15–1228:41 UT and 1228:41–1240:07 UT). Although the former time bin includes the period before the SVM front, the contribution to the accumulated particle counts would be small since the electron flux is so low in front of the SVM structure and also the fraction of the accumulation time before SVM is small (~ 2 min out of ~ 11.5 min sampling time). PA information is drawn as contour lines. Figure 9e provides the sector number and information on the looking direction of each sector for 16-sector data. For instance, sectors 1 and 2 look in the direction of the spin axis and thus these sectors detect particles moving approximately sunward (note that the direction opposite to the spin axis is deflected from Jupiterward by $\sim 20^\circ$ in the corotation direction). In Figures 9a, 9c, and 9d, significant flux peaks are seen in sectors 1 and 2, which result in the Jupiterward and corotational anisotropies ($A_{1r} < 0$ and

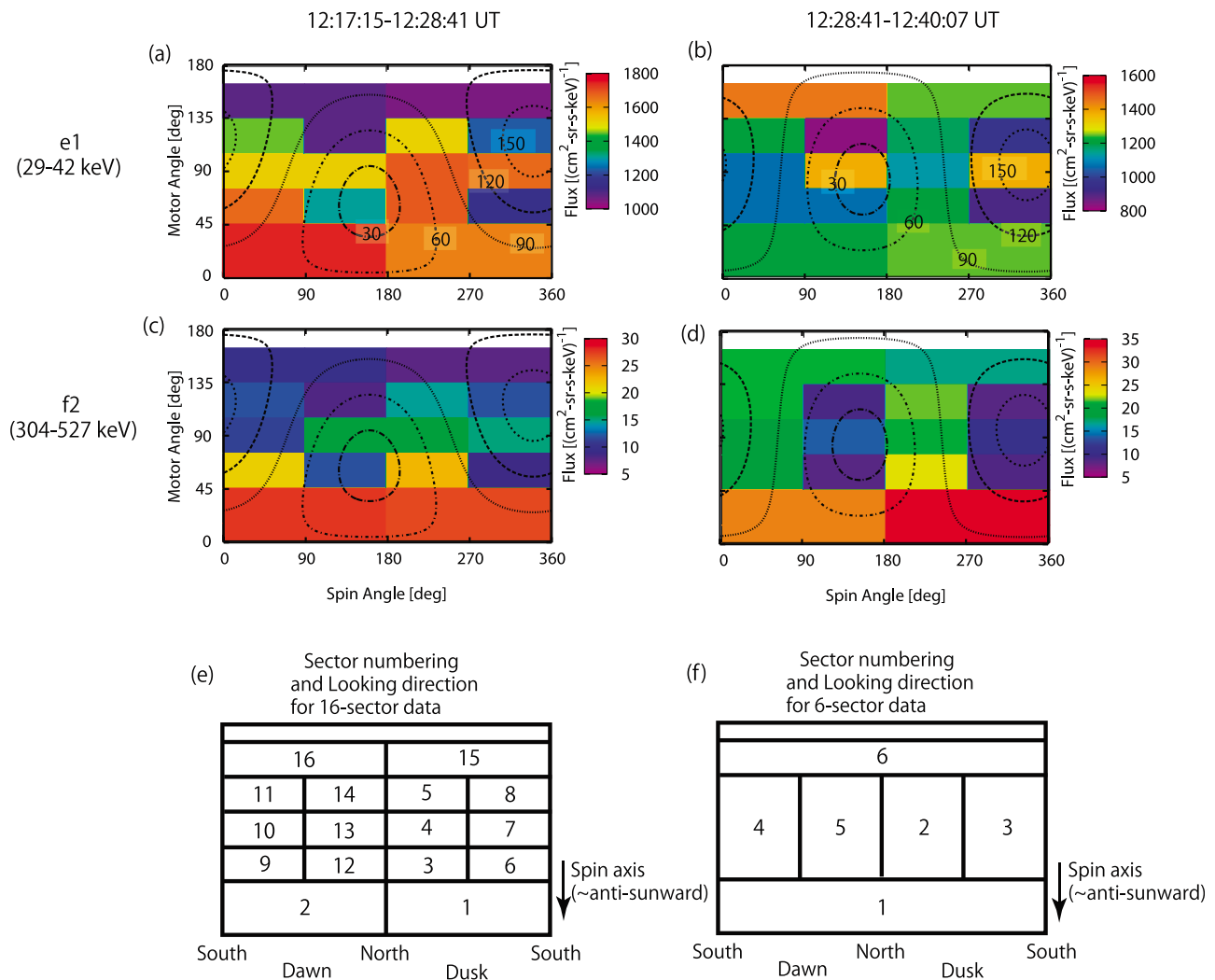


Figure 9. Angle-angle plot of energetic electron fluxes: (a) e1 flux (29–42 keV) at 1217:15–1228:41 UT, (b) e1 flux at 1228:41–1240:07 UT, (c) f2 flux (304–527 keV) at 1217:15–1228:41 UT, (d) f2 flux at 1228:41–1240:07 UT, and (e, f) sectoring information for 16-sector and 6-sector data, respectively. Note that the looking directions of sectors 1 and 2 are the spin axis direction and thus the electrons detected in these sectors are moving approximately sunward, which is deflected from the radially inward direction by $\sim 20^\circ$ in the corotation direction.

$A_{1\phi} > 0$, see Figures 6b and 6c). Sectors 1 and 2 are perpendicular to the magnetic field averaged over the EPD time bin. These plots confirm that the energetic electrons have significant anisotropy perpendicular to the magnetic field. Note also that the counting statistics are sufficient to discuss the anisotropy of $\gg 0.1$. Although not shown in the figures, the maximum and minimum counts per sampling time per sector are >10000 and >800 , respectively, for the f2 channel (304–527 keV); counts are larger in the e1 channel (29–42 keV).

[46] The Jupiterward anisotropy was absent for the e1 electrons (29–42 keV) at 1228:41–1240:07 UT, as can be seen in Figure 9b (and also in Figure 6c). This would be due to two reasons. First, the broad width of the sampling energy bin that hides the positive spectrum slope; note that even if the bulk flow exists, the anisotropy becomes zero or reversed when the spectrum slope is inverted ($\gamma < -1$), as seen in equation (4). Second, the broad width of the sampling time window (~ 11.5 min), causing the ambiguity of spectrum

slope and mixture of jet period (highly anisotropic) and non-jet period.

[47] The electron velocities for 1217:15–1228:41 UT are calculated through equation (4) and summarized in Table 1. Although it has some uncertainty, the flow is in the range of 7500 – 17000 km s^{-1} for this time period. The velocity of 7500 km s^{-1} obtained from the e1 channel is increased to 15000 km s^{-1} if we adopt the spectral index $\gamma = -0.5$ instead of $\gamma = 0$, which has significant uncertainty due to the above reasons. The electron flow velocity for the next sampling time (1228:41–1240:07 UT) can be similarly calculated to be

Table 1. Electron Parameters and Jet Velocities for ~ 1223 UT

Channel	Particle Speed	α	A_{1r}	γ	Flow Velocity V
f2	2.5×10^5 km s^{-1}	1.5	0.45	3	17000 km s^{-1}
e1	1.0×10^5 km s^{-1}	2	0.15	0 (–0.5)	7500 (15000) km s^{-1}

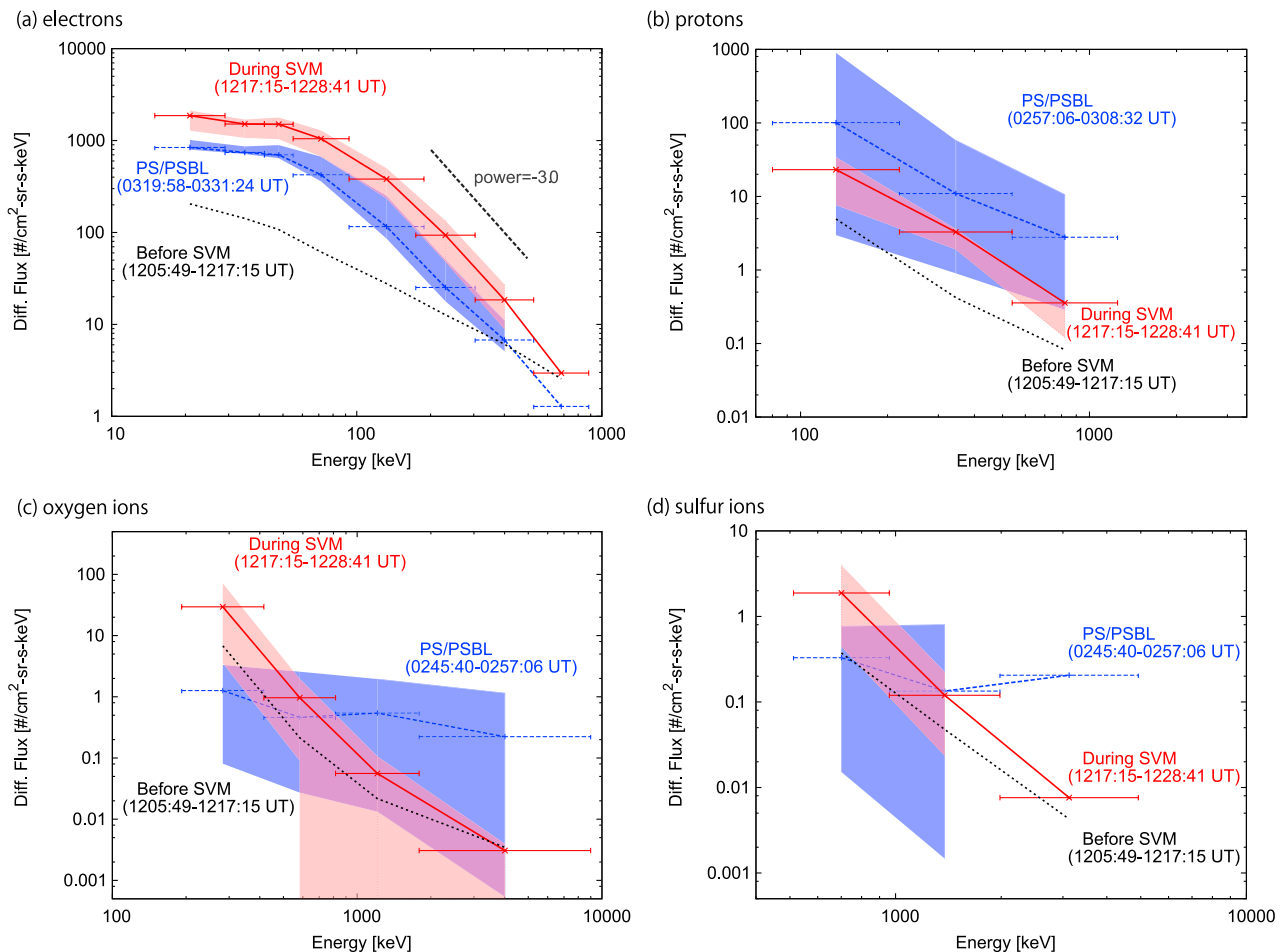


Figure 10. Energy spectra of the energetic electrons and ions. The blue curve is for fluxes in PS/PSBL (period B), and the red is for during SVM (period D). The curves are enveloped by two spectra. The top and bottom of the envelope are spectra obtained by sectors 6 and 1 for period B, respectively (indicating tailward anisotropy). For period D, top and bottom are from sectors 1 and 6, respectively (indicating Jupiterward anisotropy). Spectra just before the SVM are also displayed in black for comparison.

$\sim 7500 \text{ km s}^{-1}$ (from the f2 channel), suggesting a large-scale slow down of the electron jet or Galileo's displacement to the slow flow region. On the other hand, the ion flow velocity was $\sim 450 \text{ km s}^{-1}$, the ion Alfvén velocity was $\sim 500\text{--}650 \text{ km s}^{-1}$, and the electron Alfvén velocity was $\sim 100000 \text{ km s}^{-1}$. Therefore, the observed Jupiterward electron flow was much faster than the ion flow and the ion Alfvén velocity, whereas it is slower than the electron Alfvén velocity by an order of magnitude. The electron anisotropy became less significant well behind the SVM front (after 1245 UT).

5.4. Electron Energization

[48] Electron energization occurred associated with the SVM event. The energetic electron (omni-directional) energy spectrum during the SVM event is displayed in Figure 10a by a red solid curve and is enveloped (pink shading) by the spectra obtained by sectors 1 (top) and 6 (bottom) of the 6-sector data. The definitions of these sectors are seen in Figure 9f. Here we choose 6-sector data because 16-sector data is available only for e1 and f2 channels. The higher flux for sector 1 over the whole energy range further confirms the

significance of the electron Jupiterward flow discussed above.

[49] The electron flux significantly enhanced over the energy range below $\sim 500 \text{ keV}$ at SVM, compared to the previous sampling time (black dotted line in Figure 10a). The relativistic electrons ($>500 \text{ keV}$) also increased slightly, although the increment is much less.

[50] The spectrum during the SVM period has a shoulder at $\sim 30\text{--}40 \text{ keV}$. Although the spectral shape above the shoulder energy is not well fitted by a single power law, the slope in the sub-relativistic energy range (a few hundreds keV) is approximately represented by a spectral index of ~ 3 (gray slope).

[51] PA distributions provide significant information on the particle acceleration. Close examination of Figures 9b and 9d indicates that the e1 electrons (29–42 keV) are peaked at $\text{PA} \sim 0^\circ$ and $\sim 180^\circ$ while the f2 electrons (304–527 keV) are peaked at $\text{PA} \sim 90^\circ$. Note that the bi-directional peaks in Figure 9b were very sharp: fluxes in sectors 7 and 13 are high, while those in 6, 8, 9, 10, 12, 14, which correspond to the medium-PA, are low. On the other hand, $\text{PA} \sim 90^\circ$ flux was moderately higher than that in the medium PA.

Therefore, the obtained PA distribution might be the superposition of a pancake like distribution and a sharp bi-directional distribution.

[52] A significant increase of the electron flux was also seen in the PSBL layering structure (period B). The omnidirectional energy spectrum of the electrons is shown in Figure 10a (blue dashed curve). It is also enveloped by 6-sector flux data; the fluxes of sector 1 and 6 are at the bottom and the top, respectively, illustrating the tailward anisotropy. The spectral slope was ~ 3 . Since the electrons flowing in the PSBL probably originated from the diffusion region, the observed intense electron flux in the PSBL indicates that the acceleration in the diffusion region is also important.

5.5. Ion Energization

[53] Both acceleration sites (i.e., the SVM and the diffusion region) play significant roles in ion energization. Figures 10b–10d show the omnidirectional fluxes of the plasma sheet/PSBL (PS/PSBL) ions probably coming from the X-line (blue dashed line) and those obtained at SVM (red solid line) in the same format as the electrons. They are also enveloped by the flux obtained by sectors 1 and 6 in Figure 9f. The bottom and the top of the blue (red) envelope are the flux of the sector 1 (6) and the sector 6 (1), respectively. The differences of the flux levels between these sectors again indicate the tailward and Jupiterward anisotropies at the velocity layer and the SVM structures, respectively.

[54] Although PA anisotropies of ions in the SVM region are complex and dependent on ion species and energies, there is a tendency that the bi-directional components are significant for protons behind the SVM whereas the heavy ions around the SVM front have weaker parallel/anti-parallel components, as implied by A_{20} (Figures 6d–6f).

6. Discussion

6.1. Multiple and Recurrent X-line Formation

[55] In the simplest view of the Jovian magnetosphere by Vasyliūnas [1983], a single extended X-line is assumed. However, it is natural to expect more than one X-line to appear simultaneously or sequentially aligned in the radial direction (or Jupiter–Sun direction) and/or azimuthal direction. In fact, the duration times of energetic particle bursts are typically several tens of minutes to a few hours [Woch *et al.*, 2002], suggesting reconnection is transient and/or localized. In addition, the magnetic field deviation implies an average recurrence period of ~ 4 h [Russell *et al.*, 2000].

[56] Our close examination of energetic particle anisotropy also shows the recurrent (and possibly, simultaneously multiple) X-line formations. We identified at least three X-lines during ~ 13 h (Figure 3), and therefore the recurrence period is in agreement with that argued on the basis of the magnetic field data, ~ 4 h [Russell *et al.*, 2000]. Our observations also suggest that reconnection intermittently weakened or ceased. The duration time of each transient reconnection (e.g., the velocity layer was observed over ~ 2 – 3 h and the ion flow associated with SVM lasted ~ 0.5 – 1 h in our event) is well in the range described by Woch *et al.* [2002]. It should be noted, however, that the observed duration time would be only the lower limit of the life time, since it is ambiguous whether the observed timescale represents the passing time of an

azimuthally localized structure [e.g., Russell *et al.*, 1998; Vogt *et al.*, 2010], or the actual life time of the transient phenomena. Such spatiotemporal effects should be distinguished in future observations.

[57] Grodent *et al.* [2004] compared the above timescales to that of the nightside polar auroral spots and argued for tail reconnection as the cause of such auroral signatures. Radioti *et al.* [2011] in fact reported nearly simultaneous detection of nightside auroral spots and the magnetic field disturbance possibly due to tail reconnection. A similar relationship between reconnection and dawnside polar spots/arcs [Grodent *et al.*, 2003; Radioti *et al.*, 2008, 2010] is also expected. Although reported spots show a life time of >30 min, it has not been clear whether such spots often survive for more than several hours. More statistical studies on the duration time are required for such transient auroral signatures.

6.2. Transition to Lobe Reconnection

[58] In addition to the Vasyliūnas cycle X-line (closed field line reconnection), the Dungey cycle X-line (open field line reconnection) is also expected in the Jovian magnetotail [Cowley *et al.*, 2003]. However, observational evidence of lobe reconnection has not been well documented.

[59] In our multi-instrumental observations, initial signatures of the X-line showed evidence of a closed X-line (separatrix inside the high-density plasma sheet, see Figure 3a). About one hour later, the X-line Jupiterward of Galileo seems to have developed to an open field X-line (lobe reconnection, Figure 3b). Lobe reconnection (evident from the sharp dropout of energetic particles at the separatrix, the low electron density, and the reduced lobe magnetic field) was seen until ~ 15 UT, although some interruptions were also indicated.

[60] Transient lobe reconnection may trigger transient auroral phenomena and also plays a significant role in the (quasi-) steady Dungey cycle. Further research is important to discover how often and where such transitions to lobe reconnection occur.

[61] Although in this study we have regarded the low electron density (much lower than 10^{-2} cc $^{-1}$), the sharp boundary of the energetic particle fluxes, and the lobe field (B_r) reduction as evidences of lobe reconnection [cf. Woch *et al.*, 1999; Russell *et al.*, 2000], the connectivity of the magnetic field lines to the interplanetary field lines has not been confirmed directly. Badman and Cowley [2007] argued that the low-energy heavy ions of Jovian magnetospheric origin (i.e., oxygen ions and sulfur ions) may significantly deplete in the plasma sheet when lobe reconnection occurs. In our case, however, such depletion of heavy ions was not seen in the EPD energy range; instead, the intense fluxes (similar or more intense compared to the fluxes on previous and next days) were found in the velocity layer and the SVM structures, both of which are detected during reconnection in the extremely low-density plasma sheet. The full content of heavy ions, despite the signature of lobe reconnection, might be explained by the diffusion of plasma sheet heavy ions out to the lobe region before reconnection, as the above authors suggested. The non-adiabatic acceleration by the impulsive electric field which is especially efficient for heavy ions [Radioti *et al.*, 2007] may be responsible for the abundance of energetic heavy ions. Here we add another candidate that

Table 2. Comparison of Active Plasma Sheet Parameters Between Jupiter and Earth

	Jupiter ^a	Earth ^b
SVM front thickness	10000–20000 km	300–1000 km
Ion inertial length at SVM	13000–20000 km	300–500 km
Ion thermal gyroradius at SVM	6000–8000 km	500–600 km
Azimuthal scale of flow bursts	18–25 R_J	2–3 R_E
Electric field across flow burst region	1–3 mV/m	2 mV/m
Energy gain across flow burst region	3 MeV/q	30 keV/q

^aThe values for the SVM (top three columns) are derived in our analyses (based on the ion species of O^{2+} , S^{3+} , and O^+), whereas the values for the flow bursts (bottom three columns) are taken from *Russell et al.* [1998], *Vogt et al.* [2010], and *Kronberg et al.* [2008].

^bThe values for the SVM are adopted from the work of *Runov et al.* [2009, 2011a, 2011b] and *Sergeev et al.* [2009], whereas the values for the flow bursts are derived from the work of *Schödel et al.* [2001] and *Nakamura et al.* [2004].

explains the heavy ion content; if the Dungey cycle works significantly, heavy ions in the dayside plasma sheet can be transported with the magnetic flux tubes, which are connected to the solar wind, to the nightside lobe region, as has been suggested for the Earth's case [*Seki et al.*, 2000]. In any case, further discussion on the heavy ion distribution is difficult without the low-energy ion observations. Comprehensive investigation of the low-energy ion components in the tail plasma sheet and the lobe remain for future work.

6.3. Velocity Layer Structure Inside the Active Plasma Sheet

[62] Energetic particles are launched from the diffusion region and stream away along the magnetic field. Since the magnetic field lines convect inward (equatorward and away from the X-line), the energetic particles are also transported inward. The inward convection of the energetic particles proceeds with a common speed, while the energetic particles stream along the field line with the speed which is dependent on the energy, mass, and the PA. As a result, layering structures of energetic particles in which higher (lower)-velocity particles stream in the outer (inner) layer are formed and in fact have been observed in the Earth's magnetosphere [*Scholer et al.*, 1986; *Onsager et al.*, 1991; *Sarafopoulos et al.*, 1997].

[63] In our observations the velocity layer structure was seen associated with Jovian tail reconnection (Figure 8). The energetic particle species were electrons, protons, oxygen ions, and sulfur ions. These observations are similar to those reported by *Sarafopoulos et al.* [1997] for the terrestrial distant tail. Interestingly, these authors also noted that in some cases the electron flux peaked at the central plasma sheet rather than at the PSBL, and they argued that such a signature would be detected when the field line is closed and the electrons are trapped. According to this interpretation, our observations which represent the highest electron flux in the outer plasma sheet/PSBL and the lesser flux in the inner plasma sheet are consistent with an open field line topology (i.e., lobe reconnection).

6.4. Transient Structure Inside the Active Plasma Sheet

[64] Associated with terrestrial tail reconnection, SVM structures have often been observed in the tail region [*Nagai et al.*, 1998a; *Ohtani et al.*, 2004], and earthward-propagating

DFs have recently been analyzed by simultaneous multipoint observations [*Runov et al.*, 2009, 2011a, 2011b; *Sergeev et al.*, 2009]. These authors have revealed that DF is a kinetic structure, whose thickness is typically of the order of ion thermal gyroradius (and also the ion inertial length).

[65] The SVM event analyzed here is quite similar to the dipolarization events seen in the Earth's magnetosphere. Although this event is rather atypical in that the vertical magnetic field is stronger than the ambient horizontal field, such a rare event has also been reported in the Earth's magnetosphere [*Nagai et al.*, 1998a]. Therefore, the observed SVM is not anomalous compared to the Earth's case when we look at the qualitative features. On the other hand, the front thickness was estimated to be ~ 10000 – 20000 km, which is apparently much thicker than the Earth's case (400–500 km [*Runov et al.*, 2009], 300 km [*Sergeev et al.*, 2009], and 500–1000 km [*Runov et al.*, 2011b]; see also Table 2). Despite such a remarkable thickness, however, the observed SVM front still holds the ion-scale structure. For instance, the ion inertial length c/ω_{pi} is ~ 13000 km behind the SVM for O^{2+} or S^{3+} (~ 20000 km for O^+), which is comparable to the front thickness. Such a large inertial length compared to the Earth's case is due to the larger ion mass and lower electron density ($\omega_{pi} = \sqrt{4\pi n_e e q/m_i}$, $m_i/q \sim 10m_p/e$, $n_e \sim 0.003$ cc⁻¹). Additionally, the front thickness is not much larger than the gyroradii of streaming ions ahead of the front ($r_{gs} = m_i v_u/qB_\theta$, where v_u is the upstream ion velocity in the frame of the SVM: in this case $v_u \sim 450$ km s⁻¹). Adopting $B_\theta \sim 10$ nT and $m_i/q \sim 10m_p/e$, we obtain $r_{gs} \sim 5000$ km (if we adopt $m_i/q = 16m_p/e$, $r_{gs} \sim 8000$ km). The gyroradii of thermal ions can also be compared with the front thickness. If we assume a temperature T_i of 20 keV/q (estimated via a pressure balance in the preexisting plasma sheet and assuming that ion pressure did not change by an order of magnitude behind the SVM front) and adopting $B_\theta \sim 10$ nT (the value in the middle of the front), the thermal gyroradii (r_{gt}) are ~ 6000 km for O^{2+} and S^{3+} , and ~ 8000 km for O^+ , which are not much smaller than the front thickness.

[66] Origins of the current flowing along the front have been discussed for the Earth's case. Plasma measurements in the Earth's magnetosphere indicate that the thermal pressure gradient current of the ions and/or electrons would support the SVM structure [*Runov et al.*, 2011b; *Zhang et al.*, 2011]. In our observations, however, it is impossible to unambiguously determine the pressure gradient due to the lack of the low-energy plasma data. In the present study, we missed electrons of <15 keV, protons of <80 keV, oxygen ions of <200 keV, and sulfur ions of <500 keV; the Galileo low-energy plasma analyzer [*Frank et al.*, 1992] did not provide significant particle counts in this short time period because of the low ion density.

[67] It is also possible that ion dynamic pressure upstream (i.e., Jupiter side) of the SVM contribute to the pressure balance more than the thermal pressure does. In the frame of the SVM, upstream ions collide with the magnetic wall, resembling the situation of the magnetopause. In such a case, the electrons and/or ions deflected by the strong magnetic field support the current layer, and also the electric field in the front structure significantly affects the particle motion and hence the thickness of the layer [*Cowley*, 1995; *Parker*, 1967].

[68] As we have discussed above, the origin of the current layer supporting the SVM structure is not uniquely identified

in our observation, due to the lack of significant parameters. The ion temperature, mass, and charge state, as well as the electric field structures must be measured in the future missions in order to further investigate and understand SVM phenomena.

[69] Behind the SVM structure, the anomalously high-speed Jupiterward electron jet was observed, and its speed was much larger than the simultaneously observed ion flow velocity and the ion Alfvén velocity. A high-speed electron jet behind the SVM structure is seen in the numerical study by *Sitnov et al.* [2009] and also implied by the electric field observation [*Runov et al.*, 2011b]. Based on current simulations, however, the high-speed electron jet is confined to the region whose thickness is of the order of the electron inertial length in the vertical direction [*Fujimoto*, 2006; *Daughton et al.*, 2006; *Karimabadi et al.*, 2007; *Klimas et al.*, 2008; *Sitnov et al.*, 2009]. In our case the electron inertial length c/ω_{pe} is ~ 100 km (ω_{pe} is the electron plasma frequency), and it is unlikely for Galileo to stay in such a narrow region for a prolonged time of ~ 10 –20 min. Therefore, the observation of the high-speed electron jet by the EPD instrument, for which the particle data is averaged over the sampling time (~ 11.5 min), cannot be simply understood by the current numerical simulations. A possible interpretation is that the energetic particle flux is much more intense in the high-speed jet region compared to sparse counts in the surrounding non-jet region, and thus the averaged data over the sampling time may emphasize the anisotropy in the high-speed jet region (this may not be applied to the e1 channel, as we discussed in Section 5.3). Higher time resolution for the magnetic field and particle measurements is clearly required in order to further discuss the plasma and magnetic field structures in the active Jovian tail.

6.5. Particle Energization Mechanisms

[70] Electron acceleration mechanisms associated with magnetic reconnection have been intensively studied theoretically as well as observationally. According to simulation studies, field-aligned distributions along with the separatrix are formed by the electrons accelerated by the reconnection electric field through meandering motions in the diffusion region [*Hoshino et al.*, 2001; *Hoshino*, 2005]. Observations in the terrestrial magnetosphere show such field-aligned energetic electrons generally exist [e.g., *Nagai et al.*, 1998b; *Åsnes et al.*, 2008; *Retinò et al.*, 2008]. Energetic electrons confined to magnetic islands have also been reported [*Chen et al.*, 2008; *Retinò et al.*, 2008], as expected from simulation studies [e.g., *Drake et al.*, 2006; *Oka et al.*, 2010]. Another important acceleration site is where magnetic flux piles up and the vertical magnetic field increases [*Hoshino et al.*, 2001; *Hoshino*, 2005; *Ashour-Abdalla et al.*, 2011]. Multispacecraft observations indeed have found the energetic electrons behind the propagating DF [*Sergeev et al.*, 2009; *Ashour-Abdalla et al.*, 2011; *Runov et al.*, 2011a, 2011b].

[71] In our observations we found the energetic electrons streaming away from the X-line (probably most of them are field-aligned). A significant flux increase of the energetic electrons was also seen associated with the SVM event. We expect a pancake-like distribution for the energized electrons in an SVM structure, if they are accelerated in the direction perpendicular to the magnetic field through the betatron process around the magnetic equator. In fact the relativistic

electrons (f2, 304–527 keV) showed such a distribution (peaked around PA $\sim 90^\circ$, $A_{20} < 0$). On the other hand, lower energy electrons (e1, 29–42 keV) have a sharp field-aligned component superposed on the pancake-like distribution, as can be seen in Figure 9b. Such mixed distributions were observed in the Earth's DF [*Sergeev et al.*, 2009; *Runov et al.*, 2011a].

[72] The bi-directional accelerated component in the lower energy range (e1 channel) might be attributed to Fermi acceleration, which would result in the parallel/anti-parallel flux enhancement. In fact, a multipeak PA distribution was found in a simulation study [*Birn et al.*, 2004] and understood to be resulted from combination of the betatron process at the equator (for perpendicular acceleration) and the Fermi process (for bi-directional acceleration).

[73] Another possibility for the bi-directional component is that they are generated at another X-line within the plasma sheet Jupiterward of Galileo and streamed tailward along the field line. If this was the case, such plasma sheet (closed field line) reconnection in period D might be the seed of open field reconnection in period E, which existed Jupiterward of Galileo (Figure 3e).

[74] The energetic ions show the most enhanced fluxes at the velocity layer structure in the PS/PSBL. Field-aligned ions in the Earth's PSBL were displayed by *Hoshino et al.* [1998], whose energy exceeded the upper-limit energy of an electrostatic analyzer. In their following simulation they illustrated these PSBL ions experienced acceleration in the diffusion region via the Speiser motion. They roughly estimated the typical energy of the field-aligned ions to be about $m_i V_A^2/2$. However, the highest energies of the out-flowing ions in our observations (\sim MeV) are much higher than $m_i V_A^2/2$ (~ 1 keV/nuc for $V_A \sim 500$ km s $^{-1}$). Therefore multiple crossings of the diffusion regions and/or acceleration mechanisms other than the Speiser motion may have operated. The maximum energy gain can be estimated as the cross-tail potential gap. Assuming the electric field intensity along the X-line as $E_{XL} \sim 2$ mV/m [cf. *Kronberg et al.*, 2008] and using the inferred X-line extent of $20 R_J$ [cf. *Russell et al.*, 1998; *Vogt et al.*, 2010], keeping caution about spatiotemporal effects mentioned above in mind, the maximum energy is ~ 3 MeV/q (cf. Table 2), whereas the observed maximum ion energy was 4 MeV. In our data set, therefore, it is marginal whether additional ion acceleration mechanism is required (e.g., wave-particle interaction and/or the impulsive electric field [*Radioti et al.*, 2007]).

[75] The above maximum energy is much higher than the Earth's case. In the terrestrial magnetosphere, the cross tail voltage along the X-line can be estimated to be ~ 30 kV from the electric field of $E_{XL} \sim 2$ mV/m [*Schödel et al.*, 2001] and the width of a bursty bulk flow (BBF) $\sim 2.5 R_E$ [*Nakamura et al.*, 2004] (even if the actual X-line extent is much larger than the typical width of BBF, it is limited by the magnetospheric size as $< 40 R_E$, resulting in the maximum energy of ~ 500 keV/q). Since the typical electric field intensity is similar, the significant gap in the maximum energy which can be gained in the cross-tail drift is directly attributed to the large extent of the X-line. The Jovian tail has a clear advantage for particle acceleration, in that the cross-tail magnetospheric size, which is the approximate upper limit of the X-line extent, is ~ 100 times longer than that of the Earth. However, the actual X-line extent should be more

observationally scrutinized for Jupiter, and also theoretical effort is important to understand the factors which control the X-line extent.

7. Summary

[76] We reported the evolution of X-lines over ~ 13 h in the postmidnight sector observations on 17 June 1997. In addition to the main X-line tailward retreat, signatures of multiple/recurrent X-line formations were observed. Detailed analyses for this period showed various features in the plasma sheet. A significant density decrease was detected in the central plasma sheet, indicative of the transition to lobe reconnection, and a velocity layer structure was formed in the active plasma sheet. The strong vertical magnetic (SVM) field which is similar to a dipolarization front often seen in the Earth's tail region was also generated as a consequence of reconnection. The estimated front thickness of the SVM was close to the ion inertia length and not much larger than ion gyro radii; this is also similar to those seen in the terrestrial magnetosphere. The ion flow behind the SVM structure was close to the Alfvén velocity, while the energetic electron anisotropy suggestive of an anomalously high-speed electron jet (much higher than the ion flow) was observed. Electron and ion heating associated with these structures were also seen. All these signatures in our case study are quite similar to those observed in the Earth's magnetosphere, although the generality of such a similarity should be examined with more events. The influence of such tail activities on the planetary scale dynamics and ionospheric disturbances should also be more extensively investigated.

[77] **Acknowledgments.** The authors thank A. Lagg for providing the EPD software and useful discussions. We are also grateful to B. Kurth for the PWS data. C. M. Jackman is highly acknowledged for her useful comments on the manuscript.

[78] Philippa Browning thanks the reviewers for their assistance in evaluating this paper.

References

- Ashour-Abdalla, M., M. El-Alaoui, M. L. Goldstein, M. Zhou, D. Schriver, R. Richard, R. Walker, M. G. Kivelson, and K.-J. Hwang (2011), Observations and simulations of non-local acceleration of electrons in magnetotail magnetic reconnection events, *Nat. Phys.*, *7*, 360–365, doi:10.1038/nphys1903.
- Åsnes, A., M. G. G. T. Taylor, A. L. Borg, B. Lavraud, R. W. H. Friedel, C. P. Escoubet, H. Laakso, P. Daly, and A. N. Fazakerley (2008), Multispacecraft observation of electron beam in reconnection region, *J. Geophys. Res.*, *113*, A07S30, doi:10.1029/2007JA012770.
- Badman, S. V., and S. W. H. Cowley (2007), Significance of Dungey-cycle flows in Jupiter's and Saturn's magnetospheres, and their identification on closed equatorial field lines, *Ann. Geophys.*, *25*, 941–951, doi:10.5194/angeo-25-941-2007.
- Baker, D. N., T. I. Pulkkinen, V. Angelopoulos, W. Baumjohann, and R. L. McPherron (1996), Neutral line model of substorms: Past results and present view, *J. Geophys. Res.*, *101*, 12,975–13,010, doi:10.1029/95JA03753.
- Birmingham, T. J., and T. G. Northrop (1979), Theory of flux anisotropies in a guiding center plasma, *J. Geophys. Res.*, *84*, 41–45, doi:10.1029/JA084IA01p00041.
- Birn, J., M. F. Thomsen, and M. Hesse (2004), Electron acceleration in the dynamic magnetotail: Test particle orbits in three-dimensional magnetohydrodynamic simulation fields, *Phys. Plasmas*, *11*, 1825–1833, doi:10.1063/1.1704641.
- Chen, L.-J., et al. (2008), Observation of energetic electrons within magnetic islands, *Nat. Phys.*, *4*, 19–23, doi:10.1038/nphys777.
- Cowley, S. W. H. (1995), Theoretical perspectives of the magnetopause: A tutorial review, in *Physics of the Magnetopause*, *Geophys. Monogr. Ser.*, vol. 90, edited by P. Song, B. U. Sonnerup, and M. F. Thomsen, pp. 29–43, AGU, Washington, D. C., doi:10.1029/GM090.
- Cowley, S. W. H., E. J. Bunce, T. S. Stallard, and S. Miller (2003), Jupiter's polar ionospheric flows: Theoretical interpretation, *Geophys. Res. Lett.*, *30*(5), 1220, doi:10.1029/2002GL016030.
- Cowley, S. W. H., S. V. Badman, S. M. Imber, and S. E. Milan (2008), Comment on "Jupiter: A fundamentally different magnetospheric interaction with the solar wind" by D. J. McComas and F. Bagenal, *Geophys. Res. Lett.*, *35*, L10101, doi:10.1029/2007GL032645.
- Daughton, W., J. Scudder, and H. Karimabadi (2006), Fully kinetic simulations of undriven magnetic reconnection with open boundary conditions, *Phys. Plasmas*, *13*, 072101, doi:10.1063/1.2218817.
- Drake, J. F., M. Swisdak, H. Che, and M. A. Shay (2006), Electron acceleration from contracting magnetic islands during reconnection, *Nature*, *443*(5), 553–556, doi:10.1038/nature05116.
- Forman, M. A. (1970), The Compton-Getting effect for cosmic-ray particles and photons and the Lorentz-invariance of distribution functions, *Planet. Space Sci.*, *18*, 25–31, doi:10.1016/0032-0633(70)90064-4.
- Frank, L. A., K. L. Ackerson, J. A. Lee, M. R. English, and G. L. Pickett (1992), The plasma instrumentation for the Galileo Mission, *Space Sci. Rev.*, *60*, 283–304, doi:10.1007/BF00216858.
- Frank, L. A., W. R. Paterson, and K. K. Khurana (2002), Observations of thermal plasmas in Jupiter's magnetotail, *J. Geophys. Res.*, *107*(A1), 1003, doi:10.1029/2001JA000077.
- Fujimoto, K. (2006), Time evolution of the electron diffusion region and the reconnection rate in fully kinetic and large system, *Phys. Plasmas*, *13*, 072904, doi:10.1063/1.2220534.
- Geiss, J., et al. (1992), Plasma composition in Jupiter's magnetosphere: Initial results from the Solar Wind Ion Composition Spectrometer, *Science*, *257*, 1535–1539, doi:10.1126/science.257.5076.1535.
- Grigorenko, E. E., M. Hoshino, M. Hirai, T. Mukai, and L. M. Zelenyi (2009), "Geography" of ion acceleration in the magnetotail: X-line versus current sheet effects, *J. Geophys. Res.*, *114*, A03203, doi:10.1029/2008JA013811.
- Grodent, D., J. T. Clarke, J. Kim, J. H. Waite Jr., and S. W. H. Cowley (2003), Jupiter's main auroral oval observed with HST-STIS, *J. Geophys. Res.*, *108*(A11), 1389, doi:10.1029/2003JA009921.
- Grodent, D., J.-C. Gérard, J. T. Clarke, G. R. Gladstone, and J. H. Waite Jr. (2004), A possible auroral signature of a magnetotail reconnection process on Jupiter, *J. Geophys. Res.*, *109*, A05201, doi:10.1029/2003JA010341.
- Gurnett, D. A., W. S. Kurth, R. R. Shaw, A. Roux, R. Gendrin, C. F. Kennel, F. L. Scarf, and S. D. Shawhan (1992), The Galileo plasma wave investigation, *Space Sci. Rev.*, *60*, 341–355, doi:10.1007/BF00216861.
- Hoshino, M. (2005), Electron surfing acceleration in magnetic reconnection, *J. Geophys. Res.*, *110*, A10215, doi:10.1029/2005JA011229.
- Hoshino, M., T. Mukai, T. Yamamoto, and S. Kokubun (1998), Ion dynamics in magnetic reconnection: Comparison between numerical simulation and Geotail observations, *J. Geophys. Res.*, *103*, 4509–4530, doi:10.1029/97JA01785.
- Hoshino, M., T. Mukai, T. Terasawa, and I. Shinohara (2001), Suprathermal electron acceleration in magnetic reconnection, *J. Geophys. Res.*, *106*, 25,979–25,997, doi:10.1029/2001JA900052.
- Jackman, C. M., C. S. Arridge, H. J. McAndrews, M. G. Henderson, and R. J. Wilson (2009), Northward field excursions in Saturn's magnetotail and their relationship to magnetospheric periodicities, *Geophys. Res. Lett.*, *36*, L16101, doi:10.1029/2009GL039149.
- Karimabadi, H., W. Daughton, and J. Scudder (2007), Multi-scale structure of the electron diffusion region, *Geophys. Res. Lett.*, *34*, L13104, doi:10.1029/2007GL030306.
- Kivelson, M. G., K. K. Khurana, J. D. Means, C. T. Russell, and R. C. Snare (1992), The Galileo magnetic field investigation, *Space Sci. Rev.*, *60*, 357–383, doi:10.1007/BF00216862.
- Klimas, A., M. Hesse, and S. Zenitani (2008) Particle-in-cell simulation of collisionless reconnection with open outflow boundaries, *Phys. Plasmas*, *15*, 082102, doi:10.1063/1.2965826.
- Krimigis, S. M., and E. C. Roelof (1983), Low-energy particle population, in *Physics of the Jovian Magnetosphere*, edited by A. J. Dessler, 106–156, Cambridge Univ. Press, Cambridge, U. K.
- Kronberg, E. A., J. Woch, N. Krupp, A. Lagg, K. K. Khurana, and K.-H. Glassmeier (2005), Mass release at Jupiter: Substorm-like processes in the Jovian magnetotail, *J. Geophys. Res.*, *110*, A03211, doi:10.1029/2004JA010777.
- Kronberg, E. A., J. Woch, N. Krupp, and A. Lagg (2008), Mass release process in the Jovian magnetosphere: Statistics on particle burst parameters, *J. Geophys. Res.*, *113*, A10202, doi:10.1029/2008JA013332.
- Kronberg, E. A., S. Kasahara, N. Krupp, and J. Woch (2011), Field-aligned beams and reconnection in the Jovian magnetotail, *Icarus*, doi:10.1016/j.icarus.2011.10.011, in press.

- Krupp, N., J. Woch, A. Lagg, B. Wilken, S. Livi, and D. J. Williams (1998), Energetic particle bursts in the predawn Jovian magnetotail, *Geophys. Res. Lett.*, *25*, 1249–1252, doi:10.1029/98GL00863.
- Krupp, N., A. Lagg, S. Livi, B. Wilken, J. Woch, E. C. Roelof, and D. J. Williams (2001), Global flows of energetic ions in Jupiter's equatorial plane: First-order approximation, *J. Geophys. Res.*, *106*, 26,017–26,032, doi:10.1029/2000JA900138.
- Kurth, W. S. (1992), Continuum radiation in planetary magnetospheres, in *Planetary Radio Emissions III*, edited by H. O. Rucker et al., pp. 329–350, Austrian Acad. of Sci. Press, Vienna.
- Louarn, P., A. Roux, S. Perraut, W. S. Kurth, and D. A. Gurnett (2000), A study of the Jovian “energetic magnetospheric events” observed by Galileo: Role in the radial plasma transport, *J. Geophys. Res.*, *105*, 13,073–13,088, doi:10.1029/1999JA900478.
- McComas, D. J., and F. Bagenal (2007), Jupiter: A fundamentally different magnetospheric interaction with the solar wind, *Geophys. Res. Lett.*, *34*, L20106, doi:10.1029/2007GL031078.
- Nagai, T., M. Fujimoto, M. S. Nakamura, R. Nakamura, Y. Saito, T. Mukai, T. Yamamoto, A. Nishida, and S. Kokubun (1998a), A large southward magnetic field of -23.5 nT in the January 10, 1995, plasmoid, *J. Geophys. Res.*, *103*, 4441–4451, doi:10.1029/97JA02449.
- Nagai, T., M. Fujimoto, Y. Saito, S. Machida, T. Terasawa, R. Nakamura, T. Yamamoto, T. Mukai, A. Nishida, and S. Kokubun (1998b), Structure and dynamics of magnetic reconnection for substorm onsets with Geotail observations, *J. Geophys. Res.*, *103*, 4419–4440, doi:10.1029/97JA02190.
- Nakamura, R., et al. (2004), Spatial scale of high-speed flows in the plasma sheet observed by Cluster, *Geophys. Res. Lett.*, *31*, L09804, doi:10.1029/2004GL019558.
- Nishida, A. (1983), Reconnection in the Jovian magnetosphere, *Geophys. Res. Lett.*, *10*, 451–454, doi:10.1029/GL010i006p00451.
- Ohtani, S., M. A. Shay, and T. Mukai (2004), Temporal structure of the fast convective flow in the plasma sheet: Comparison between observations and two-fluid simulations, *J. Geophys. Res.*, *109*, A03210, doi:10.1029/2003JA010002.
- Øieroset, M., R. P. Lin, T. D. Phan, D. E. Larson, and S. D. Bale (2002), Evidence for electron acceleration up to ~ 300 keV in the magnetic reconnection diffusion region of Earth's magnetotail, *Phys. Rev. Lett.*, *89*, 195001, doi:10.1103/PhysRevLett.89.195001.
- Oka, M., M. Fujimoto, I. Shinohara, and T. D. Phan (2010), “Island surfing” mechanism of electron acceleration during magnetic reconnection, *J. Geophys. Res.*, *115*, A08223, doi:10.1029/2010JA015392.
- Onsager, T. G., M. F. Thomsen, R. C. Elphic, and J. T. Gosling (1991), Model of electron and ion distributions in the plasma sheet boundary layer, *J. Geophys. Res.*, *96*, 20,999–21,011, doi:10.1029/91JA01983.
- Parker, E. N. (1967), Confinement of a magnetic field by a beam of ions, *J. Geophys. Res.*, *72*, 2315–2322, doi:10.1029/JZ072i009p02315.
- Pritchett, P. L. (2006), Relativistic electron production during driven magnetic reconnection, *Geophys. Res. Lett.*, *33*, L13104, doi:10.1029/2005GL025267.
- Radioti, A., J. Woch, E. A. Kronberg, N. Krupp, A. Lagg, K.-H. Glassmeier, and M. K. Dougherty (2007), Energetic ion composition during reconfiguration events in the Jovian magnetotail, *J. Geophys. Res.*, *112*, A06221, doi:10.1029/2006JA012047.
- Radioti, A., D. Grodent, J.-C. Gérard, B. Bonfond, and J. T. Clarke (2008), Auroral polar dawn spots: Signatures of internally driven reconnection processes at Jupiter's magnetotail, *Geophys. Res. Lett.*, *35*, L03104, doi:10.1029/2007GL032460.
- Radioti, A., D. Grodent, J.-C. Gérard, and B. Bonfond (2010), Auroral signatures of flow bursts released during magnetotail reconnection at Jupiter, *J. Geophys. Res.*, *115*, A07214, doi:10.1029/2009JA014844.
- Radioti, A., D. Grodent, J.-C. Gérard, M. F. Vogt, M. Lystrup, and B. Bonfond (2011), Nightside reconnection at Jupiter: Auroral and magnetic field observations from 26 July 1998, *J. Geophys. Res.*, *116*, A03221, doi:10.1029/2010JA016200.
- Retinò, A., et al. (2008), Cluster observations of energetic electrons and electromagnetic fields within a reconnecting thin current sheet in the Earth's magnetotail, *J. Geophys. Res.*, *113*, A12215, doi:10.1029/2008JA013511.
- Runov, A., V. Angelopoulos, M. I. Sitnov, V. A. Sergeev, J. Bonnell, J. P. McFadden, D. Larson, K.-H. Glassmeier, and U. Auster (2009), THEMIS observations of an earthward-propagating dipolarization front, *Geophys. Res. Lett.*, *36*, L14106, doi:10.1029/2009GL038980.
- Runov, A., et al. (2011a), Dipolarization fronts in the magnetotail plasma sheet, *Planet. Space Sci.*, *59*, 517–525, doi:10.1016/j.pss.2010.06.006.
- Runov, A., V. Angelopoulos, X.-Z. Zhou, X.-J. Zhang, S. Li, F. Plaschke, and J. Bonnell (2011b), A THEMIS multicase study of dipolarization fronts in the magnetotail plasma sheet, *J. Geophys. Res.*, *116*, A05216, doi:10.1029/2010JA016316.
- Russell, C. T. (2000), How northward turnings of the IMF can lead to substorm expansion onsets, *Geophys. Res. Lett.*, *27*, 3257–3259, doi:10.1029/2000GL011910.
- Russell, C. T., K. K. Khurana, D. E. Huddleston, and M. G. Kivelson (1998), Localized reconnection in the near Jovian magnetotail, *Science*, *280*, 1061–1064, doi:10.1126/science.280.5366.1061.
- Russell, C. T., K. K. Khurana, M. G. Kivelson, and D. E. Huddleston (2000), Substorms at Jupiter: Galileo observations of transient reconnection in the near tail, *Adv. Space Res.*, *26*, 1499–1504, doi:10.1016/S0273-1177(00)00084-3.
- Sarafopoulos, D. V., E. T. Sarris, V. Angelopoulos, T. Yamamoto, and S. Kokubun (1997), Spatial structure of the plasma sheet boundary layer at distances greater than 180 R_E as derived from energetic particle measurements on GEOTAIL, *Ann. Geophys.*, *15*, 1246–1256, doi:10.1007/s00585-997-1246-0.
- Schödel, R., W. Baumjohann, R. Nakamura, V. A. Sergeev, and T. Mukai (2001), Rapid flux transport in the central plasma sheet, *J. Geophys. Res.*, *106*, 301–313, doi:10.1029/2000JA900139.
- Scholer, M., D. N. Baker, G. Gloeckler, B. Klecker, F. M. Ipavich, T. Terasawa, B. T. Tsurutani, and A. B. Galvin (1986), Energetic particle beams in the plasma sheet boundary layer following substorm expansion: Simultaneous near-Earth and distant tail observations, *J. Geophys. Res.*, *91*, 4277–4286, doi:10.1029/JA091iA04p04277.
- Seki, K., R. C. Elphic, M. F. Thomsen, J. Bonnell, E. J. Lund, M. Hirahara, T. Terasawa, and T. Mukai (2000), Cold flowing O⁺ beams in the lobe/mantle at Geotail: Does FAST observe the source?, *J. Geophys. Res.*, *105*, 15,931–15,944, doi:10.1029/1999JA900470.
- Sergeev, V., V. Angelopoulos, S. Apatenkov, J. Bonnell, R. Ergun, R. Nakamura, J. McFadden, D. Larson, and A. Runov (2009), Kinetic structure of the sharp injection/dipolarization front in the flow-braking region, *Geophys. Res. Lett.*, *36*, L21105, doi:10.1029/2009GL040658.
- Sitnov, M. I., M. Swisdak, and A. V. Divin (2009), Dipolarization fronts as a signature of transient reconnection in the magnetotail, *J. Geophys. Res.*, *114*, A04202, doi:10.1029/2008JA013980.
- Terasawa, T., and A. Nishida (1976), Simultaneous observations of relativistic electron bursts and neutral-line signatures in the magnetotail, *Planet. Space Sci.*, *24*, 855–866, doi:10.1016/0032-0633(76)90076-3.
- Vasyliūnas, V. M. (1983), Plasma distribution and flow, in *Physics of the Jovian Magnetosphere*, edited by A. J. Dessler, pp. 395–453, Cambridge Univ. Press, Cambridge, U. K.
- Vogt, M. F., M. G. Kivelson, K. K. Khurana, S. P. Joy, and R. J. Walker (2010), Reconnection and flows in the Jovian magnetotail as inferred from magnetometer observations, *J. Geophys. Res.*, *115*, A06219, doi:10.1029/2009JA015098.
- Williams, D. J., R. W. McEntire, S. Jaskulek, and B. Wilken (1992), The Galileo Energetic Particles Detector, *Space Sci. Rev.*, *60*, 385–412, doi:10.1007/BF00216863.
- Woch, J., et al. (1999), Plasma sheet dynamics in the Jovian magnetotail: Signatures for substorm-like processes?, *Geophys. Res. Lett.*, *26*, 2137–2140, doi:10.1029/1999GL900493.
- Woch, J., N. Krupp, and A. Lagg (2002), Particle bursts in the Jovian magnetosphere: Evidence for a near-Jupiter neutral line, *Geophys. Res. Lett.*, *29*(7), 1138, doi:10.1029/2001GL014080.
- Zhang, X.-J., V. Angelopoulos, A. Runov, X.-Z. Zhou, J. Bonnell, J. P. McFadden, D. Larson, and U. Auster (2011), Current-carriers near dipolarization fronts in the magnetotail: A THEMIS event study, *J. Geophys. Res.*, *116*, A00I20, doi:10.1029/2010JA015885.

S. V. Badman, M. Fujimoto, S. Kasahara, T. Kimura, and C. Tao, Institute of Space and Astronautical Science, Japan Aerospace Exploration Agency, Yoshinodai 3-1-1, Chuo-ku, Sagami-hara 252-5210, Japan. (kshr@stp.isas.jaxa.jp)

E. A. Kronberg and N. Krupp, Max-Planck-Institut für Sonnensystemforschung, Max-Planck-Str. 2, D-37191 Katlenburg-Lindau, Germany.

A. Retinò, Laboratoire de Physique des Plasmas-CNRS, Observatoire de Saint-Maur, 4 avenue de Neptune, F-94107 Saint-Maur-Des-Fossés, France.